Available online at www.sciencedirect.com
ScienceDirect
Journal of Sound and Vibration 298 (2006) 982–1000
JOURNAL OF SOUND AND VIBRATION
www.elsevier.com/locate/jsvi

On the efficiency of screens near roadside cuttings

A.T. Peplow*

Marcus Wallenberg Laboratory for Sound and Vibration Research, Department of Aeronautics & Vehicle Engineering, Kungliga Tekniska Högskolan (KTH), S-100 44, Stockholm, Sweden

Received 3 August 2005; received in revised form 1 June 2006; accepted 1 June 2006
Available online 31 July 2006

Abstract

The prediction of acoustic propagation from a monofrequency coherent line source in a cutting with impedance boundary conditions over a noise-screen onto surrounding flat grassland is presented. It is well known that over flat ground the spectra for single-noise screens have significant marked differences for propagation over absorbing ground where the screen obstructs surface wave attenuation over the absorbing ground cover. The aim here is to extend the study of this phenomenon for screens adjacent to cuttings or dips surrounded by absorbing ground. The study is based on a numerical model using boundary element techniques that enables the excess attenuation and insertion loss for various noise barriers and cuttings of complex profile and surface cover to be calculated. The model is applied to single-foundation noise barriers to which additional absorbent or rigid side-panels are added to create profiles and a double-barrier configuration is also studied. Spectra of insertion loss, change in insertion loss and excess attenuation results for a broadband traffic-source are presented. It is concluded that "multiple-edged" barriers only show a minor increase in acoustic efficiency over simple vertical screens for a noise source located in perturbed flat ground conditions such as a cutting; in addition it is shown that a screen placed close to the source shows sign of partial improvement.

1. Introduction

A boundary integral equation formulation for the two-dimensional Helmholtz equation in a locally perturbed half-plane has been developed to calculate sound propagation out of a cutting of arbitrary cross-section and surface impedance over a road-side noise barrier onto surrounding flat homogeneous ground [1], see Fig. 1, and results from simulations are considered. Specifically, the case considered is that of propagation from a monofrequency coherent line source in a cutting which is assumed to be straight and infinitely long with cross-section and surface treatment that do not vary along its length. The noise barrier lies in the plane and it is assumed the axis of the barrier and cutting are parallel to the axis of the source and the impedance is allowed to vary in the cutting and around the barrier obstacle in the plane perpendicular to the line source. So that, it is possible to model, for example, a road running down the centre of the cutting, with grassy banks and noise barriers on either side.

Our discussion and numerical scheme is limited throughout to the case of a coherent line source of sound, which has the advantage that the mathematical problem is two-dimensional so that the computational

*Fax: +46 8 7906122.
E-mail address: atpeplow@kth.se.

0022-460X/$ - see front matter © 2006 Elsevier Ltd. All rights reserved.
doi:10.1016/j.jsv.2006.06.022

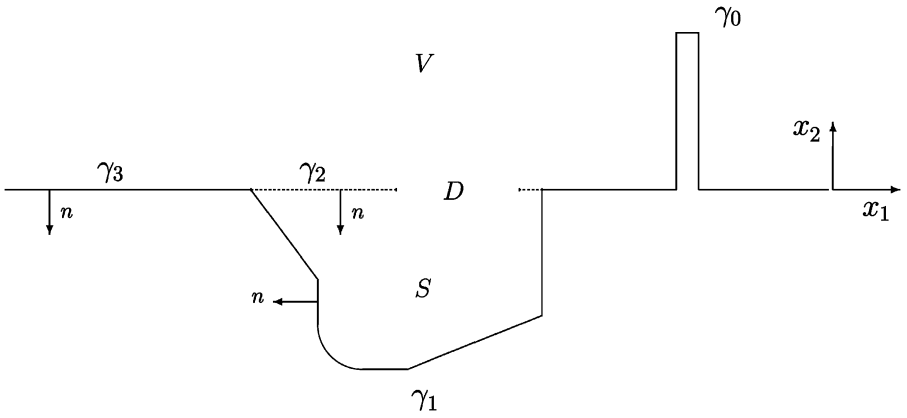

Fig. 1. Geometry of the model.

problem is feasible. A traffic noise stream is more realistically modelled as an incoherent line source, especially as regards calculation of L_{eq} values, and a single vehicle is more realistically modelled as a point source of sound. Both these cases, via partial Fourier transformation, can be reduced to the solution of a sequence of two-dimensional problems with a coherent line source of sound which can then be treated using the formulation and numerical scheme we describe: see Duhamel [2] or Chandler-Wilde [3] for details.

A related problem is the case when the cutting (γ_1) is not present and the problem lies entirely within the upper half-plane V. This case has been used as a model of acoustic propagation over outdoor noise barriers (see e.g. Ref. [4]). In this case a formulation as a single integral equation over γ_0 is possible using the impedance Green's function for the upper half-plane V as fundamental solution. This approach fails when γ_1 lies below the upper half-plane V since this Green's function is undefined at points outside V. For a recent general review of the application of boundary integral equation methods in modelling outdoor noise problems see Refs. [3,5], for interference-type multi-edge profiles [6–8] and Refs. [9,10] for the problem without a noise screen.

The numerical method of solution of the boundary integral equations implemented is a product integration method using the product mid-point rule and has been presented in detail in Ref. [1]. Predictions of attenuation and insertion losses, are presented for a traffic noise spectrum for site configurations where the traffic noise is propagating out of a cutting and onto surrounding flat ground. To illustrate the scope of the mathematical model we make calculations examining the effect on the excess attenuation of the depth of the cutting and of various configurations of the noise barrier.

The article is outlined as follows. Section 2 describes the formulation of the boundary value problem (BVP) in the unbounded domain and he boundary integral equations formulated, derived from the BVP via applications of Green's second theorem in U and S. For $\beta_c \neq 0$ (a complex frequency-dependent admittance value representing soft or grassland), we use as the fundamental solution in the upper half-plane V the Green's function G_{β_c} (given in the next section) for the Helmholtz equation with impedance boundary condition of constant admittance β_c on the boundary ∂U. The integral equation formulation is a coupled system of four integral equations, three second-kind Fredholm equations and one first-kind Fredholm equation. Section 3 presents the results from applying the numerical method to the barrier on flat ground case and the barrier adjacent to a road-side cutting. A short sub-section, regarding various barrier/source scenarios, considers the characterisation of physical mechanisms that may cause such degradation in barrier insertion loss. Some general comments regarding barrier location and design conclude the article in Section 4.

2. The boundary integral equation method

A numerical method has been developed which enables the wave field for various noise screens/cuttings/ground type to be calculated. The numerical model is two-dimensional with a point source of sound and the

coordinates of the corners of the cutting and barrier cross-section are input as data for the model. Surface characteristics of the barrier, in terms of the acoustic impedance, are defined independently for each segment of the cross-section. In three dimensions, the model accurately describes effects of a coherent line source of sound parallel to the configuration of infinite length, constant cross-section and constant distribution of surface cover along its length. While the modelled situation is unrealistic in absolute sound pressure levels, the predictions of changes in insertion loss are valuable for a variety of screen shapes, ground surfaces and source environments.

Given a source at x_0 somewhere in the region D, the pressure induced at x, denoted by $p(x)$ (a harmonic time dependence e^{-iwt} is assumed and suppressed throughout), may be written as the sum of the incoming field and the scattered field, that is $p(x) = G_f(x, x_0) + P(x)$ where $G_f(x, x_0) := -\frac{i}{4}H_0^{(1)}(k|x - x_0|)$ ($H_0^{(1)}$ the Hankel function of the first-kind of order zero and k the wavenumber) is the free-field Green's function. The pressure p is assumed to satisfy the following BVP:

Given a wavenumber $k > 0$ and an impedance over the ground, β, such that β is constant ($= \beta_c$) on γ_3, the flat surface, find p such that

$$p(x) = P(x) + G_f(x, x_0), \quad x \in \overline{D}\backslash\{x_0\}, \tag{1}$$

and such that p satisfies the Helmholtz equation

$$(\nabla^2 + k^2)p(x) = 0, \quad x \in D\backslash\{x_0\}, \tag{2}$$

the impedance boundary condition,

$$\frac{\partial p}{\partial n}(x) = ik\beta(x)p(x), \quad x \in \partial D, \tag{3}$$

and the Sommerfeld radiation conditions

$$\partial p(x)/\partial r - ikp(x) = o(r^{-1/2}), \tag{4}$$

uniformly in x as $r := |x| \to \infty$ and $n(x)$ denotes the normal directed out of the fluid medium as shown in Fig. 1. The normal at the interface, γ_2 is assumed to be directed into the volume, S.

We denote by $G_{\beta_c}(x, x_0)$ the fundamental solution to the Helmholtz equation in $\overline{V}$ which satisfies the Sommerfeld radiation conditions (4) and the impedance boundary condition $\partial G_{\beta_c}(x, x_0)/\partial n(x) = ik\beta_c G_{\beta_c}(x, x_0)$ on $x \in \partial V$.

Analytical expressions for $G_{\beta_c}(x, x_0)$ have been obtained by Rasmussen [12], Filippi [13] (and see Ref. [14]), and by Chandler-Wilde and Hothersall [11]. From Ref. [11] we have that, for $x, x_0 \in \overline{V}$, $x \neq x_0$,

$$G_{\beta_c}(x, x_0) = G_f(x, x_0) + G_f(x, x_0') + P_{\beta_c}(k(x - x_0')),$$

where x_0' is the image of x_0 in the x_1-axis and, for $-\infty < \xi < +\infty$, $\eta \geqslant 0$, $\beta_c \neq 1$, $P_{\beta_c}((\xi, \eta))$ is given by

$$P_{\beta_c}((\xi, \eta)) = \frac{\beta_c e^{i\rho}}{\pi}\int_0^\infty t^{-1/2}e^{-\rho t}g(t)\,dt + \frac{\beta_c e^{i\rho(1-a_+)}}{2\sqrt{1-\beta_c^2}}\,\mathrm{erfc}(e^{-i\pi/4}\sqrt{\rho a_+}) \tag{5}$$

with $\rho = (\xi^2 + \eta^2)^{1/2}$, $\gamma = \eta/\rho$, $a_+ = 1 + \beta_c\gamma - \sqrt{1-\beta_c^2}\sqrt{1-\gamma^2}$, erfc the complementary error function, and

$$g(t) = \frac{-\beta_c - \gamma(1 + it)}{\sqrt{t - 2i(t^2 - 2i(1 + \beta_c\gamma)t - (\beta_c + \gamma)^2)}} - \frac{e^{-i\pi/4}\sqrt{a_+}}{2\sqrt{1-\beta_c^2}(t - ia_+)}.$$

(Note that all the complex square roots in the above expressions are to be taken with non-negative real part.) The above formulae for $G_{\beta_c}(x, x_0)$ are used for all the numerical calculations reported later in this paper. The integral in Eq. (5) can be evaluated efficiently and accurately by Gauss–Laguerre quadrature as described and analysed in Ref. [11].

The numerical approach uses the boundary element method applied to a boundary integral equation similar to the Kirchoff–Helmholtz integral equation. In formulating the integral equations over the domains S and V, Fig. 1, the Green function for propagation over a homogeneous plane is used as the fundamental solution in V [11] and the free-field Green function for volume S. The integrals extend only over the screen, the cutting

interface and the cutting boundary. Then, the following system has been derived in Ref. [1]:

$$\varepsilon_0(x)p(x) = \int_{\gamma_2} G_{\beta_c}(x,y)\left(\mathrm{i}k\beta_c p(y) - \frac{\partial p(y)}{\partial n}\right)\mathrm{d}s(y) + \int_{\gamma_0}\left(\frac{\partial G_{\beta_c}(x,y)}{\partial n(y)} - \mathrm{i}kG_{\beta_c}(x,y)\beta(y)\right)p(y)\,\mathrm{d}s(y) + \eta(x_0)G_{\beta_c}(x,x_0), \quad x \in \overline{V}\backslash\{x_0\}, \tag{6}$$

where

$$\eta(x_0) = \begin{cases} 1, & x_0 \in V, \\ 0, & x_0 \in S, \end{cases}$$

and $\varepsilon_0(x) = 1$, $x \in V \cup \gamma_2$, $\varepsilon_0(x) = 0$, $x \in \mathsf{R}^2\backslash\overline{V}$, and $\varepsilon_0(x) = 1/2$ on the obstacle, $x \in \gamma_0$ away from corner points

and

$$\varepsilon_1(x)p(x) = \int_{\gamma_2}\left(G_f(x,y)\frac{\partial p(y)}{\partial n} - \frac{\partial G_f(x,y)}{\partial n(y)}p(y)\right)\mathrm{d}s(y) + \int_{\gamma_1} p(y)\left(\frac{\partial G_f(x,y)}{\partial n(y)} - \mathrm{i}k\beta(y)G_f(x,y)\right)\mathrm{d}s(y) + (1-\eta(x_0))G_f(x,x_0), \quad x \in \overline{S}\backslash\{x_0\}, \tag{7}$$

where $\varepsilon_1(x) = 1$, $x \in S$, $\varepsilon_1(x) = 0$, $x \in \mathsf{R}^2\backslash\overline{S}$, and $\varepsilon_1(x) = \frac{1}{2}$ at points $x \in \partial S$ which are not corner points.

Eqs. (6) and (7) express the pressure in D in terms of the unknowns p and $\partial p/\partial n$ on γ_2, p on γ_1, and p on γ_0. The unknowns for a boundary element solution are $p_0 := p|_{\gamma_0}$, $p_1 := p|_{\gamma_1}$, $p_2 := p|_{\gamma_2}$ and $q := \mathrm{i}k\beta_c p_2 - \partial p/\partial n|_{\gamma_2}$.

The integral over the boundary surfaces can be evaluated numerically once the unknowns pressure p_0, p_1, p_2 and q have been calculated. These values can be determined by solving Eqs. (6) and (7) by a standard boundary element technique involving the solution of a set of linear equations to determine the values at points which are the nodes of the boundary elements. Piecewise constant functions are used as basis functions and collocation takes place at mid-sided nodes thus avoiding corner points. In the practical implementation, the coordinates of the corners of the barrier and cutting are input as data for the model, and the surface characteristics in the form of the acoustic admittance of each linear surface segment can be defined separately. Predictions for barrier/cutting/sources on mixed ground can be made by including sections of the ground in the definition of the barrier cross-section and assigning the appropriate surface characteristics. The coding is organised so that closed, discrete parts of the cross-section do not need to be in contact with the ground surface, and this feature is used to model diffraction around the multiple-edged barrier designs described in this paper. The boundary elements defined on the boundary surfaces have lengths ranging from 0.01λ for the low frequencies to 0.1λ for the highest frequencies, where λ is the wavelength of the source. This provides good resolution of the screen and cutting shape and a sufficiently accurate solution. For short wavelengths, large barriers and long cuttings/highways the expense in terms of computing time and storage to solve the problem can be considerable. For conditions typical of those described later, running on a Pentium IV Desktop, the program might take about 4 min of CPU time to run. A more detailed description of the method and its approximation is given in Ref. [1]. The coherent line source configuration modelled is not a practical one, as in reality a number of different vehicles along the length of a road will contribute to the noise field at a position behind the barrier (approximating an incoherent line source). However, the results can be related to practical measurements. Specifically, the numerical model predictions of insertion loss, at a particular frequency and receiver position, agree very well with insertion loss results for a point source of sound. The point source is located on the same line as the line source, and in the same vertical plane as the receiver, perpendicular to the barrier. To confirm this observation, comparisons have been made [6,15] with insertion loss spectra for point sources of sound, obtained from other numerical models, model experiments in an anechoic chamber and outdoor experiments, for a variety of barrier cross-sections. Results are presented in terms of the excess attenuation (EA), or insertion loss (IL), defined by $\mathrm{EA} = 20\log(P_f/P_c)$ and $\mathrm{IL} = 20\log(P_g/P_c)$ where P_f, is the free-field pressure at the receiver for the given source position, P_g is the pressure at the receiver with the flat ground/cutting/highway present, and P_c, is the pressure with both ground/cutting/highway and barrier present.

Generally, the pressure was calculated at third octave centre frequencies between 63 and 3162 Hz. Results with and without the barrier produce insertion loss spectra for the barrier in question. The attenuation of a barrier for a broadband noise source, with a spectrum representative of A-weighted road traffic noise (Sollentuna, Sweden [16]), was also obtained at each of the receiver positions by combining the calculated results at third octave centre frequencies for propagation with and without the presence of the barrier. The effect of this combination is to smooth out the complicated interference effects occurring in the spectra for receiver positions above the ground and are presented as contour diagrams.

3. Results

We show in this section some results illustrating the use of the piecewise constant collocation numerical method to simulate traffic noise propagating out of a cutting, over a noise barrier and onto surrounding flat ground, and consider results illustrating the effect of the cutting topography in later sub-sections.

Fig. 2 shows the geometries that were used in the model, unless otherwise stated. In (a)(I) a 2.0 m high vertical screen with rigid surfaces and a width of 0.2 m was positioned 5.81 m from the source. The Origin located at the bottom-centre of the barrier as shown in Fig. 2(a)(I). This is the fundamental barrier design over which all other positions of screens are considered as modifications of this basic scenario where the source is located 0.5 m above the road surface. A variation of the basic configuration is shown in Fig. 2(b), where a shorter barrier is positioned so that the line of sight from the source to the corner of the rear barrier (a) grazed it's upper edge. It was assumed that this screen would be located 1.0 m from the source, the minimum distance a screen is allowed from the source. For screen (b), it can be seen that at this distance from the source, its height becomes 0.76 m. The noise reduction effects of shallow road cuttings have been of some interest in the UK, see Ref. [10], here we do not study a full model of a cutting but a representative geometry in order to draw some basic conclusions. Fig. 2 also shows the geometry of the cutting. The cutting being 2.4 m wide at the top and, modelling a single carriageway, 1.5 m wide along the lower surface. The source located 1.0 m from the bottom right corner. The depth of the cutting was varied from 0.4 to 1.0 m. The surface type was the same on the ground surface outside the cutting as on the sides of the cutting. The floor of the cutting was kept rigid. The admittance used for the ground surface and sides of the cutting was that predicted by the Delany and Bazley formula [17] with an effective flow resistivity of $\sigma = 250,000\,\mathrm{N\,s\,m^{-4}}$ and depth, $D = 0.1\,\mathrm{m}$, values appropriate to grassland.

An important feature of the numerical method is that the ground surface or any linear segment in any position on the barrier, can be given different absorbing qualities. The numerical model makes the assumption that the material is locally reacting and, to describe the barrier surface impedance, the empirical model of Delaney and Bazley [17] for fibrous material is used with a flow resistivity of $20,000\,\mathrm{N\,s\,m^{-4}}$ and a layer depth 0.1 m. For the results shown the admittance β_c of the absorbing ground is calculated using the Delany and Bazley formulae. These can be related to the normal incidence energy absorption coefficient, which is a commonly quoted parameter for such materials. The absorption coefficients for the treatments described are plotted in Fig. 3 as a function of frequency.

Fig. 4 shows the spectra of insertion loss values for a special case for flat absorbent ground, Fig. 2(a)(I) and(b)(I), represented previously in the article [15], Fig. 7. The source/barrier configuration differing in this work, specifically the receiver position located $(40, 0.0)$ and source situated at $(-5.81, 0.0)$, but the trends in Ref. [15], Fig. 7 are comparative. A striking observation is apparent in the Fig. 2(a)(I) case where the insertion loss becomes negative above 1000 Hz. For the shorter, closer screen Fig. 2(b)(I) this effect is shifted to a higher frequency 1800 Hz. Placing absorbent material on the front face of the screen produces only a marginal improvement in each case, the closer screen improving by about 1.5 dB through the frequency range (solid markers in Fig. 4). For a single barrier over hard ground a general trend of increasing insertion loss with frequency has been observed previously, Ref. [15]. This is not true here as the ground-reflected wave absorption minimum has been obstructed by the introduction of a screen. Some improvement over this phenomena is possible if screens (a) and (b) are combined as multiple-noise barriers as studied extensively in Ref. [15]. Fig. 4 shows a consistent improvement over the frequency range shown in the figure, namely the insertion loss remaining positive. The improvement by introducing material on the front faces of each barrier is not consistent throughout which may be accounted for by multiple reflections occurring between the

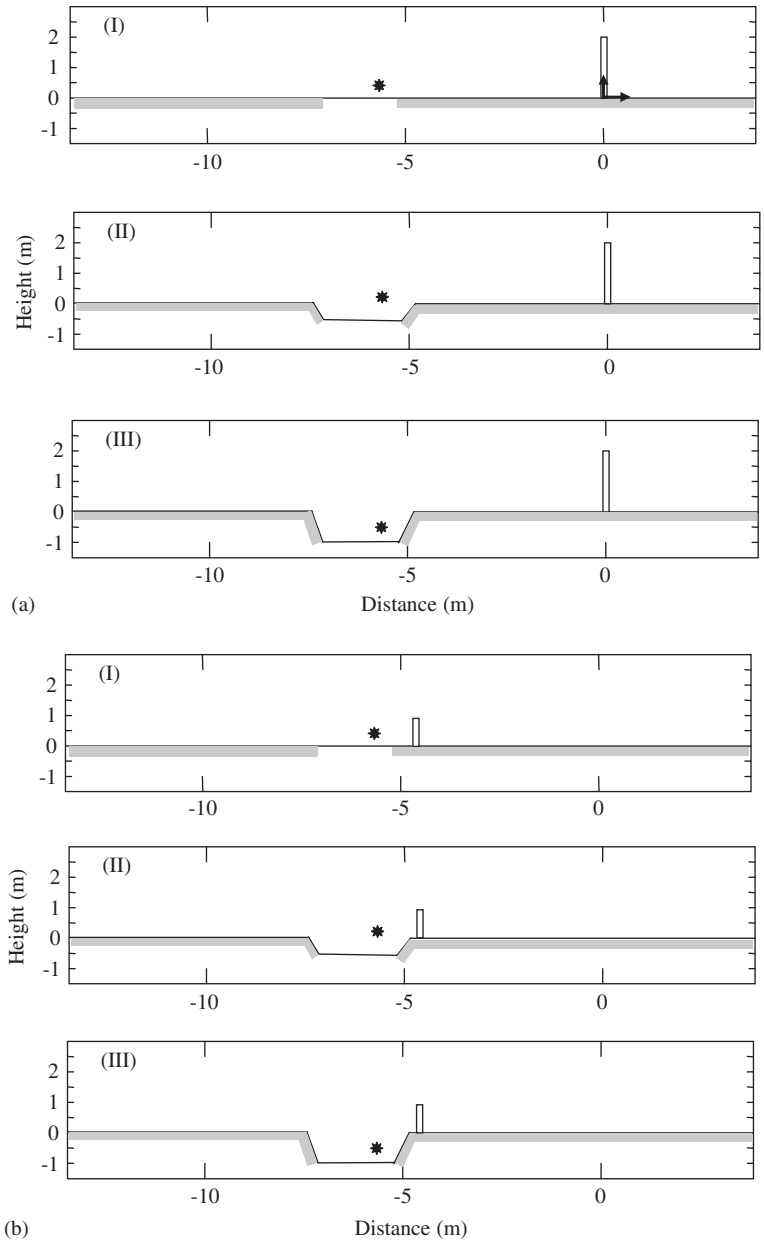

Fig. 2. Diagram of limited configurations including single 2.0 m barrier, centred at the Origin (indicated by solid arrows in (a)(I)), on grassland with source located 5.81 m from centre of screen sitting on 1.5 m wide roadway, (a)(I). Cuttings of depth 0.4 and 1.0 m are also shown as are configurations with a short, close barrier 0.76 m high, 4.8 m to the left of the origin, in (b),(I),(II), and (III). Absorbent materials may also be placed on source-facing panels.

screens. It seems that adding an additional screen to the overall configuration improves the insertion loss favourably. This raises an issue when an extra variable of a topography is included in the model and is the subject of the rest of the article.

3.1. Propagation out of a cutting

Before the study of insertion loss for screens adjacent to cuttings or dips attenuation over the ground beyond the perturbation is necessary. Fig. 2 shows the geometry used (excluding the screen). A source was

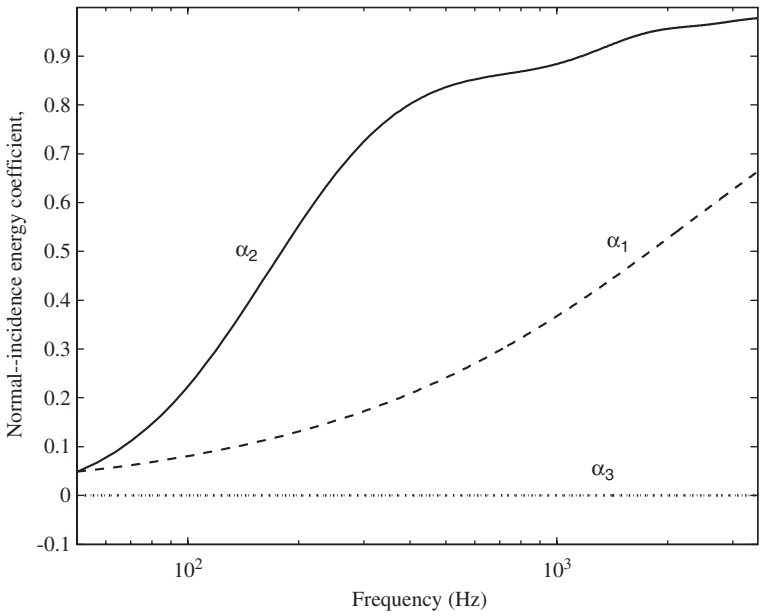

Fig. 3. Normal incidence energy absorption coefficient as a function of frequency for different surface treatments; α_1, flow resistivity 250 000 N s m^{-4}, layer depth = 0.1 m (grassland); α_2, flow resistivity 20 000 N s m^{-4}, layer depth = 0.1 m (mineral wool); and α_3, flow resistivity 10^{20} N s m^{-4}, layer depth = 0.0 m (rigid).

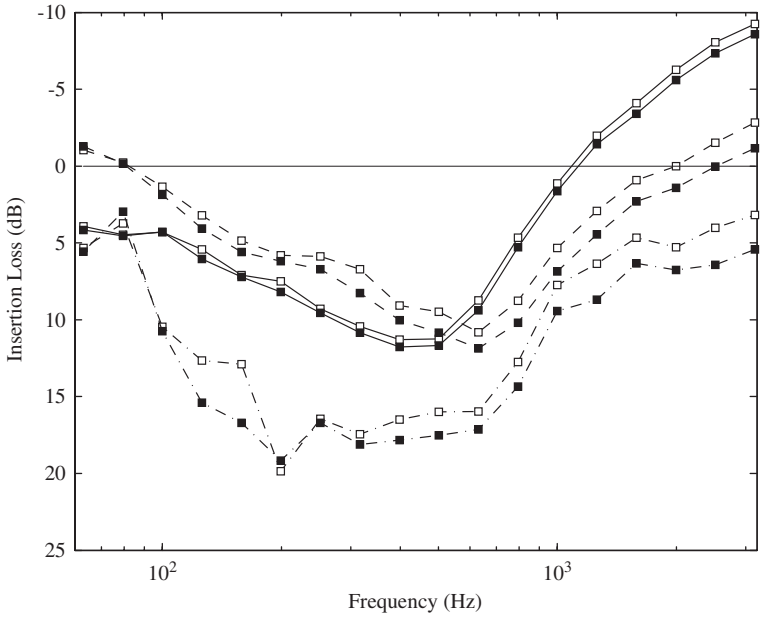

Fig. 4. Spectral analysis of the effects of absorptive treatment and absorbing ground on a single barrier Fig. 2(a)(I) or (b)(I) and double barrier (a)(I) combined with (b)(I). The receiver position located 45.0 m from barrier (a), resting on ground surface and source 5.81 m left of barrier located in ground surface also. Squares (□) with solid lines (–) denote single barrier (a)(I); dashed lines (- -) single barrier (b)(I); and dash-dot lines (-.) denote combined barriers (a) and (b) results. Solid markers (■) denote absorptive surface treatment (on source facing panels) results, respectively.

placed, in all cases, 0.5 m off the rigid floor of a 1.5 m wide cutting. The depth of the symmetric cutting was varied from 0.0, 0.4 to 1.0 m separated from the upper half-space by 2.4 m wide interface. The cutting was chosen for its simplified geometry and size so the computational study was not inhibited by problem size. The

two depths, 0.4 and 1.0 m were chosen to represent a medium- and steep-sided geometry. Note that the source position in the former case was located deliberately above the flat-ground. A third cutting depth, 0.1 m, representing a shallow perturbation from flat ground, was also studied with similar results to the 0.4 m cutting case. The type of ground was the same on the surface of the ground and on the sides of the cutting. The admittance used for the ground surface and sides of the cutting was that predicted by the Delany and Bazley formula [17] with a flow resistivity appropriate to grassland. It is seen in Fig. 5 that there is a decrease in level above that in free-field conditions, beyond 800 Hz, in each case at receiver position (40, 1.5) significantly the final case where there is no direct wave from source to receiver. However, at other receiver positions contours of broad band excess attenuation results are given Fig. 6, which are predictions for a single vehicle, A-weighted, road traffic noise spectrum, see Table 1. These are calculated by finding the attenuation of each third octave centre frequency between 63 and 3162 Hz.

In Fig. 7, a spectral analysis of the insertion loss at one receiver position for combinations of barriers and cuttings is presented as detailed in Fig. 2 with the source located 0.5 m above the road surface. It must be noted here that results at this location are fairly representative for all receiver positions between 20 and 80 m distance from origin. The solid lines represent insertion loss for vertical, rigid barriers over flat ground, case (a)(I) and (b)(I). It is clear that in the flat ground case insertion loss stays positive. However, similar to the case shown in Fig. 4, when a source is located over a dip (a)(II–III) and (b)(II–III) insertion loss strays negative at around 800 and 1200 Hz for (a)(II) and (b)(II), respectively, whereas for a deeper cutting dominant parts of the insertion loss becomes negative at 400 and 900 Hz for (a)(III) and (b)(III). These results may be caused by, in the location of the barrier, the path difference between the direct wave and the wave reflected from the rigid floor of the cutting (carriageway). This is large ($\geqslant 1.0$ m) so that there is a rapid fluctuation between constructive and destructive interferences at single frequencies. Therefore it will be more meaningful to calculate the insertion loss and excess attenuation over a broadband traffic noise spectrum. This is highlighted, for cases (a)(I–III), in Fig. 8, showing contours of excess attenuation over free-field conditions for the broad band traffic noise spectrum. The complex nature of sound attenuation with the presence of the barrier is evident on comparison with attenuations shown in Fig. 6 where an increase in attenuation by a few decibels as the cutting depth increases is observed. However, in the presence of the barrier attenuation *decreases* as cutting

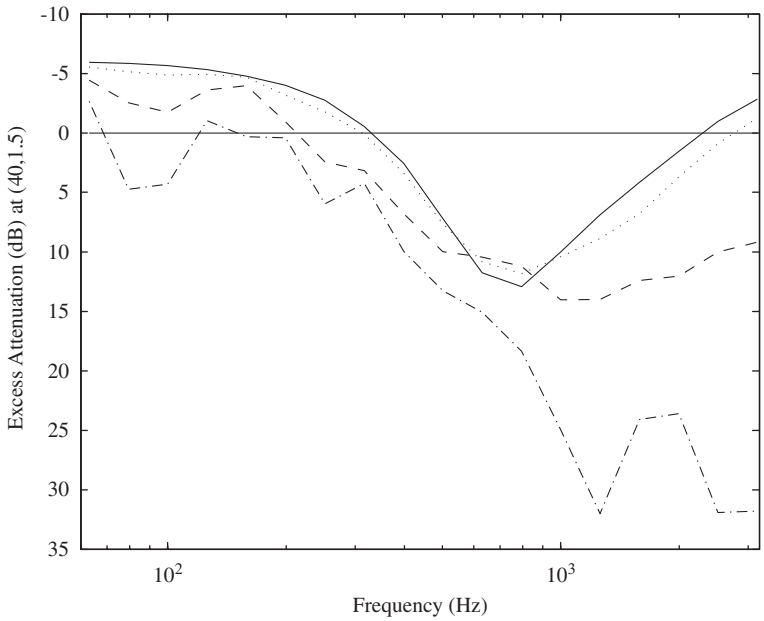

Fig. 5. Spectral analysis of excess attenuation at receiver position (40.0, 1.5) over four configurations without noise screen; Fig. 2(I),(II) or (III) including an extra solution for shallow cutting 0.1 m deep. Solid lines (–) represent flat ground results, dotted line (···) 0.1 m deep cutting, dashed line (- -) 0.4 m cutting and dash-dot line (-.) represents 1.0 m cutting results.

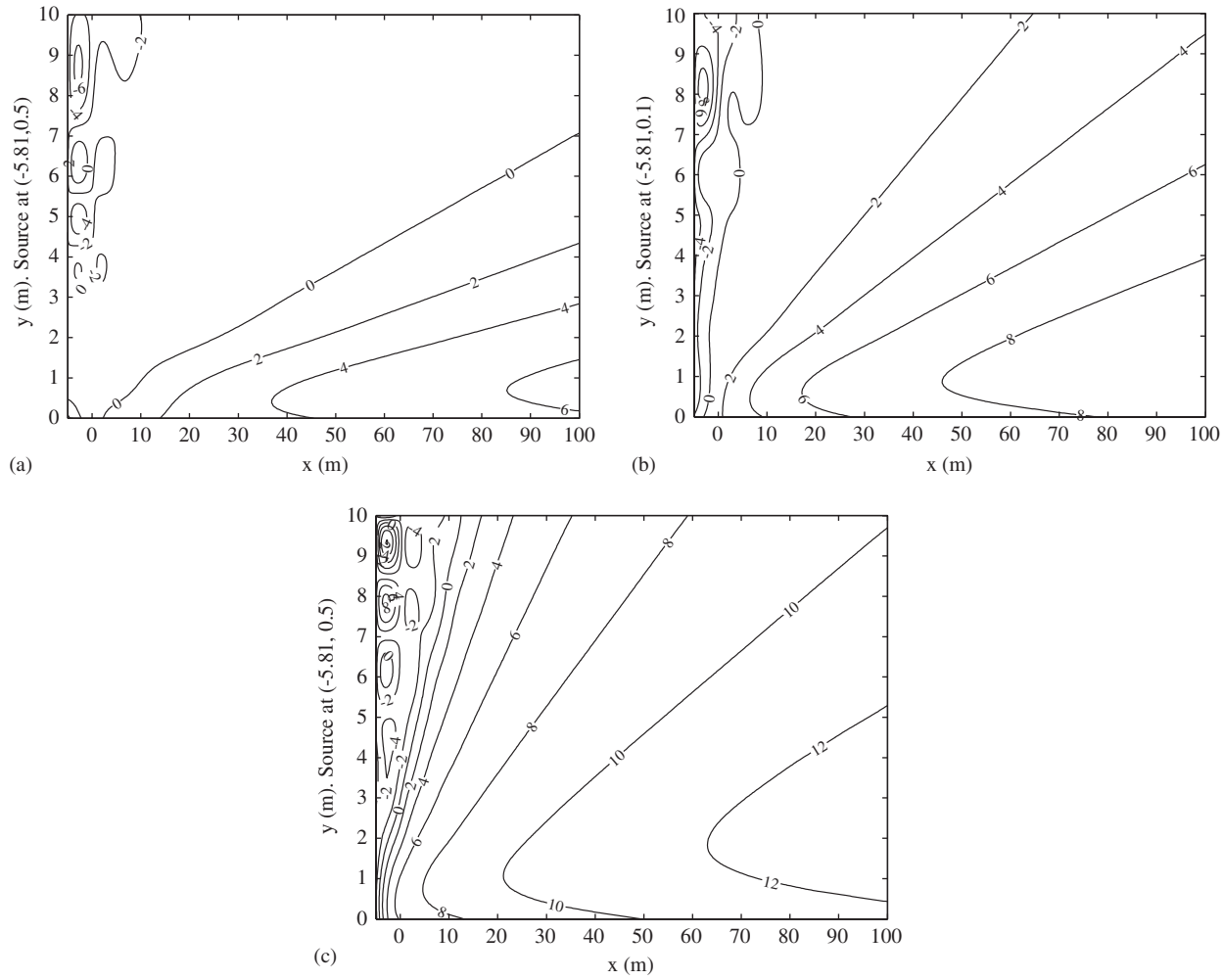

Fig. 6. Contours of excess attenuation beyond source and cutting (without screens) for broadband noise, (a) flat-ground (including rigid highway), (b) cutting 0.4 m deep, and (c), cutting 1.0 m deep.

depth increases. Thus an effective negative insertion loss is inevitable in the receiver range and barrier design prescribed here. Nevertheless, noise screen design may have a positive effect on changes in insertion loss using effective retrospective measures that could be applied relatively easily to barriers already in existence.

3.2. Cutting and single-barrier designs

Results from the previous section show that there is a significant change in the physics of the problem if a source is located in a cutting perturbation compared to sound propagation attenuation over flat grassland. The cutting changes the source characteristics significantly especially if the source is located within the cutting or in its immediate vicinity. In addition the sides and edges of the cutting create an extra screening effect which may disturb the shadowing or diffraction qualities of a noise barrier. These two effects are not easily quantifiable but the following show the overall qualitative behaviour.

First, the source was located at the bottom of a 0.4 m cutting and each screen was located so that the line-of-sight from the source to the upper corner of the cutting grazed the edge of the screen. With reference to Fig. 9, it can be seen that if a barrier is placed at a distance 1.0 m from the cutting, its height becomes 0.4 m. This

Table 1
A-weighted road traffic noise from measurements carried out at Sollentuna, Sweden in 1996 at third octave centre frequencies

Frequency (Hz)	Source strength (dB)
63.1	50.3
79.4	48.0
100.0	43.3
125.8	42.7
158.5	47.2
199.5	89.8
251.2	50.0
316.2	51.7
398.1	55.0
501.2	60.0
631.0	60.9
794.3	64.0
1000.0	66.1
1259.0	64.2
1584.9	62.0
1995.3	60.2
2511.9	58.8
3162.3	53.6

The speed was 70 km/h and the traffic mix was 10–15% heavy vehicles [16].

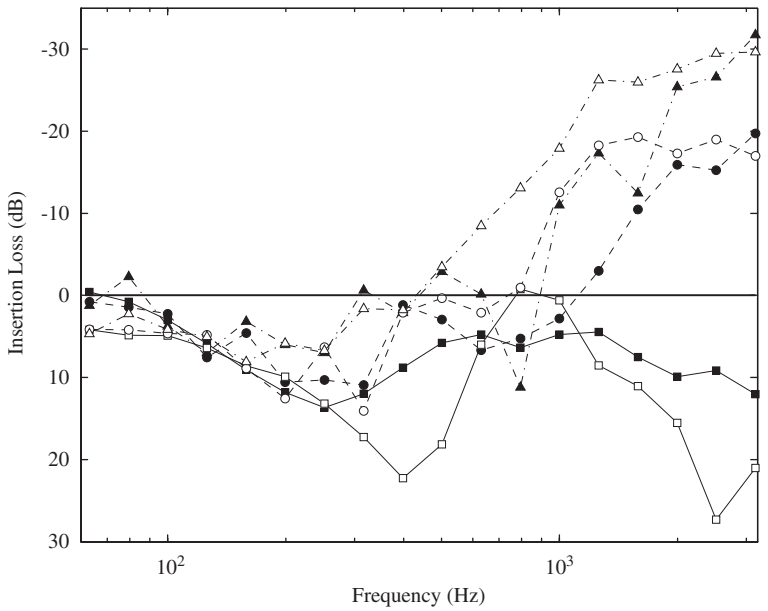

Fig. 7. Spectral analysis of insertion loss results for barrier combinations, Fig. 2(a),(I–III) and short screen (b),(I–III). The receiver position is 40.0 m from the origin 1.5 m above ground surface. Lines with square (□), circle (○), and triangle (△) markers represent results for barrier (a) on flat ground, barrier adjacent to 0.4 m cutting, and barrier adjacent to 0.9 m cutting, respectively. Solid markers denote respective results for barrier (b).

ensures that while studying the relative efficiency of screens of varying height, the shortest unobstructed path between the source and the receiver positions remained constant. The different screens (1)–(6) have the same effective height where the closest screen has height of 0.05 m. The excess attenuation for each barrier design were calculated at three receiver locations (20, 0), (40, 0), and (80, 0) all in the ground surface,

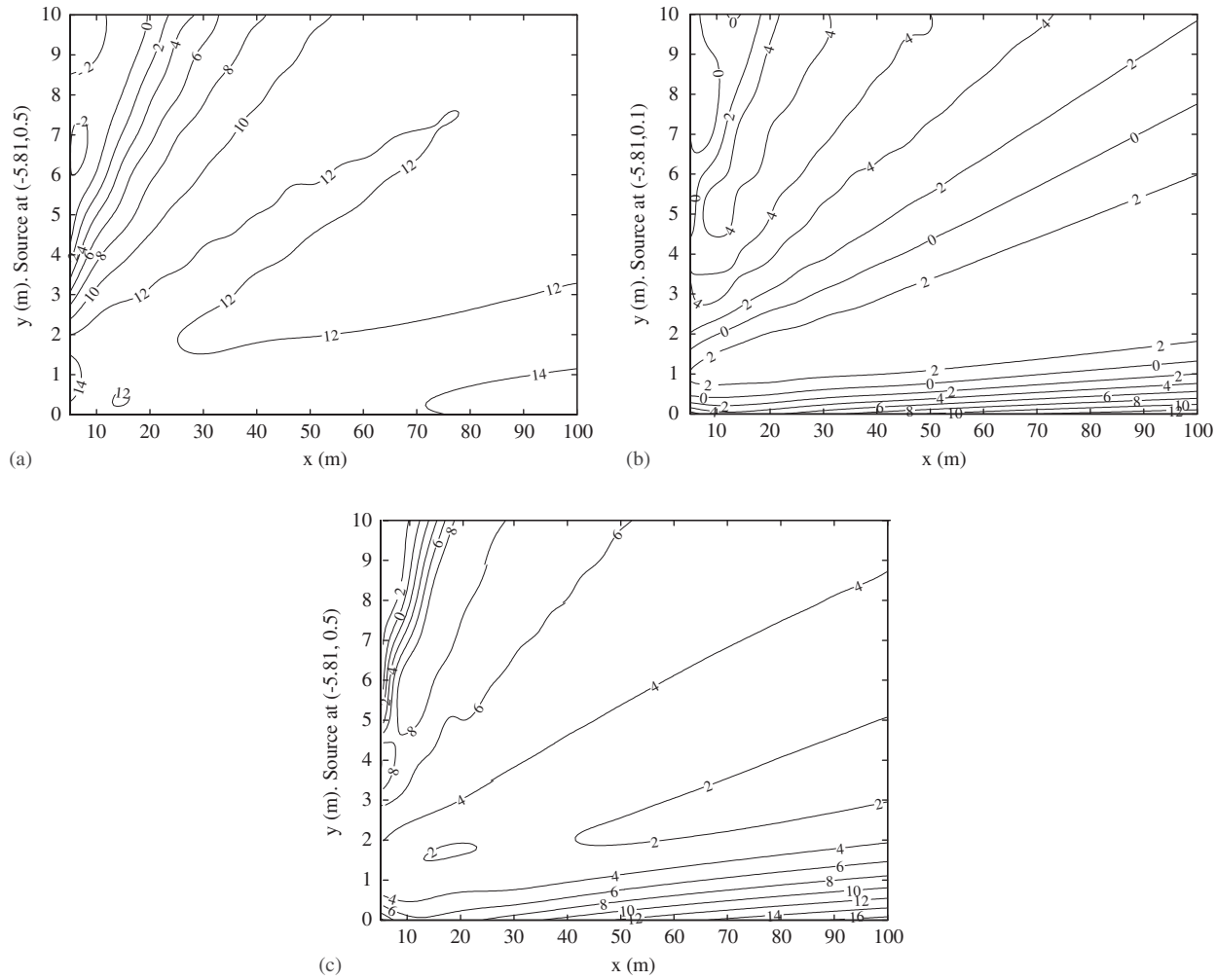

Fig. 8. Contours of excess attenuation beyond source (with 2.0 m vertical screen, Fig. 2(a)) and cutting for broadband noise, (a) flat-ground (including rigid highway), (b) cutting 0.4 m deep, and (c), cutting 1.0 m deep.

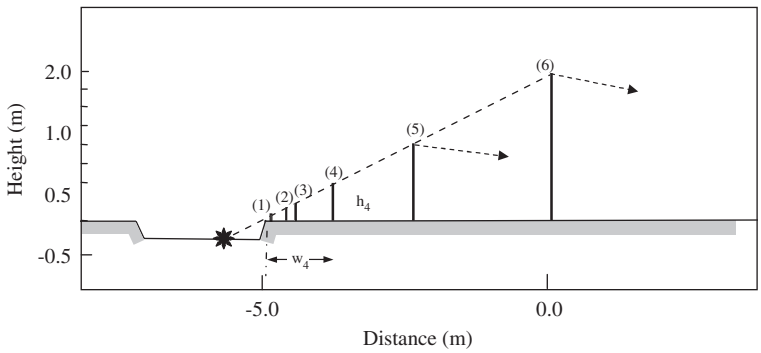

Fig. 9. Geometries for six individual screens along the line-of-sight between source and upper cutting edge, showing distance ($w_4 = 1.0$ m) and height ($h_4 = 0.4$ m) for the fourth barrier. Other distances and heights are: $w_1 = 0.05$ m, $h_1 = 0.02$ m; $w_2 = 0.25$ m, $h_2 = 0.10$ m; $w_3 = 0.50$ m, $h_3 = 0.20$ m; $w_5 = 2.50$ m, $h_5 = 1.00$ m; and $w_6 = 5.00$ m, $h_6 = 2.00$ m. The cutting depth is 0.4 m.

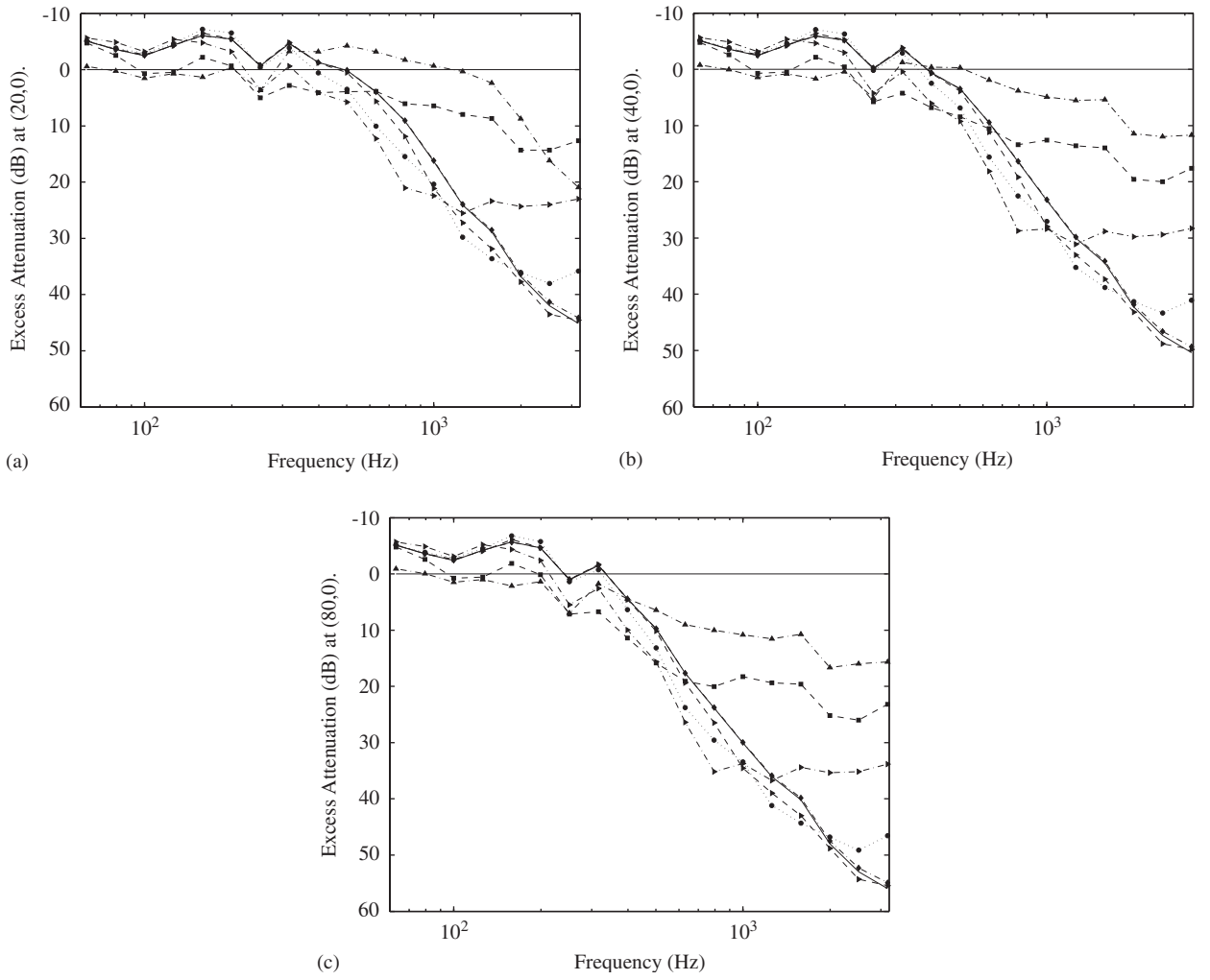

Fig. 10. Excess attenuation due to source on ground for cutting of depth 0.4 m (5.81 m from Origin, see Fig. 9) at three receiver positions also located on the ground. Barrier location and height varied for line-of-sight grazing with edge of cutting Fig. 9; (a) receiver (20, 0), (b) receiver (40, 0), and (c) receiver at (80, 0). Solid line (–) represents results over 0.4 m cutting without barrier; dotted line (···) with solid circle represents barrier(1) results; dash-dot (-.) line with marker (◆) represents barrier(2); dashed (- -) line with marker (▶), barrier(3); dash-dot (-.) line with marker (▶), barrier(4); dashed(3) (- -) line with marker (■), barrier(5); and dash-dot (-.) line with marker (▲), barrier(6) results.

and shown in Fig. 10. When the source and receiver and the receiver are above the ground the form of the spectrum of the excess attenuation is complicated due to interference between direct, ground-reflected rays and reflections in the cutting. It is clear from Fig. 10(a), there is a certain frequency (or wavelength) for which excess attenuation decreases. This is due to the ground effect between cutting and the receiver being disrupted. For barrier (6) it is 2.0 kHz, barrier (5) 500 Hz and barrier (4) a decrease in excess attenuation occurs beyond 300 Hz. For the closer barriers (1)–(3) there is little or no ground degradation between the cutting and the screen. Similar conclusions may be drawn for positions at 40 and 80 m in Fig. 10(b) and (c).

Secondly, to remove the influence of the source within the local cutting perturbation, the position of the source was located further from the road-cutting configuration. With reference to Fig. 2 it is clear that this is not a model for a highway. With the source located at $(-10.81, 0.5)$ insertion loss values will represent the

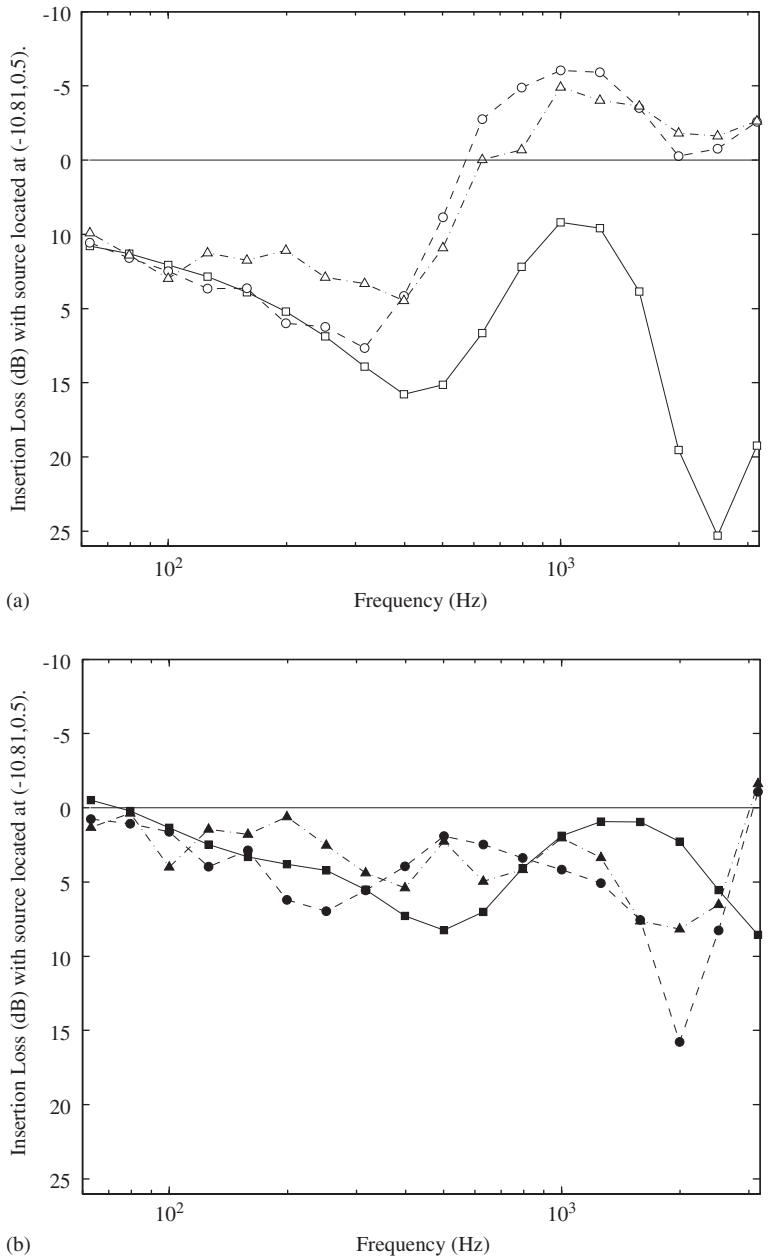

Fig. 11. Insertion loss results for single-barrier combinations, Fig. 2(a),(I–III) and short screen (b),(I–III). The receiver position is 40 m from the origin, 1.5 m above ground surface and source is located to the left of the cutting above the ground surface, at $(-10.81, 0.5)$. In upper plot lines with (□), (○) and (△) markers represent results for single barrier (a)(I), (a)(II), and (a)(III) respectively. In lower plot solid markers denote respective results for barriers (b) in Fig. 2.

qualitative effect of a small perturbation from the flat-ground case and results were considered at one receiver position $(40.0, 1.5)$. From Fig. 11 it is evident that values of insertion loss degraded significantly for case (a), independent of cutting depth at a wavelength close to 1.5 m. Whereas for a short screen close to the barrier, Fig. 11(b), only a minor change is evident. This shows that a combination of a cutting and disruption of ground effect does degrade the overall screening effect of a barrier.

Adding an extra small noise screen close to the cutting (as in Fig. 2) is a possible solution for traffic noise reduction. Furthermore, lightweight, inexpensive, reflective panels could easily be incorporated on to vertical barriers with little extra expense or alteration in foundation design. This is the subject of the next section.

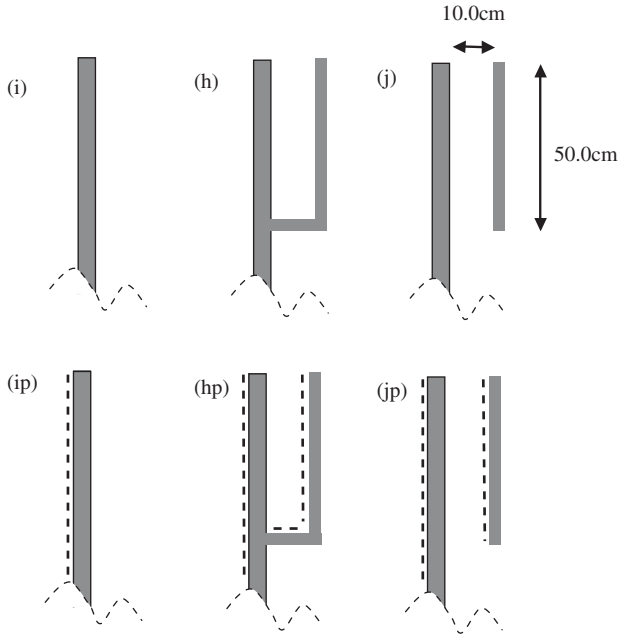

Fig. 12. Geometrical details for multi-edged barrier examples. Dashed lines in (ip), (jp), and (hp) denote absorptive treatments, α_2, see Fig. 3.

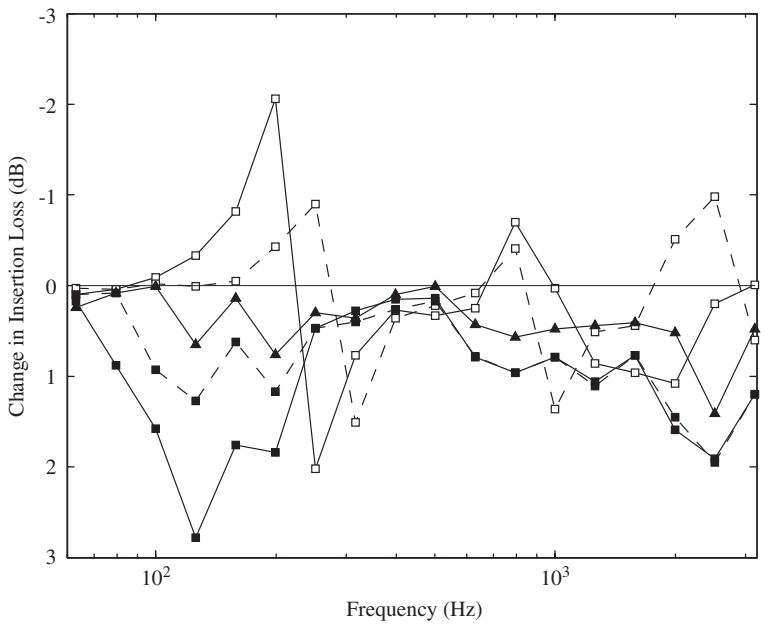

Fig. 13. Spectral comparison of different multiple-edge barrier designs over flat ground. Key indicated in Fig. 12. Results are presented in terms of the change in insertion loss compared with a vertical, rigid barrier, design (a)(I) in Fig. 2. Solid line (–) with marker (□) denotes results for (h) modification; marker (□) with dashed line (- -) denotes (j) modification results; (▲) with solid line denotes (ip) results; (■) with solid line (–) denotes (hp) results; and (■) with dashed line (- -) denotes (jp) results.

3.3. Cutting and extended barrier designs

In the following simulations the geometry of the screen design is modified by adding panels or absorbing surfaces as shown in Fig. 12. Fig. 13 shows comparisons for barriers, on flat ground, (h) and (j) against design (i) (design (a)(I) in Fig. 2) the results indicate that joining a panel to the main screen with a horizontal section

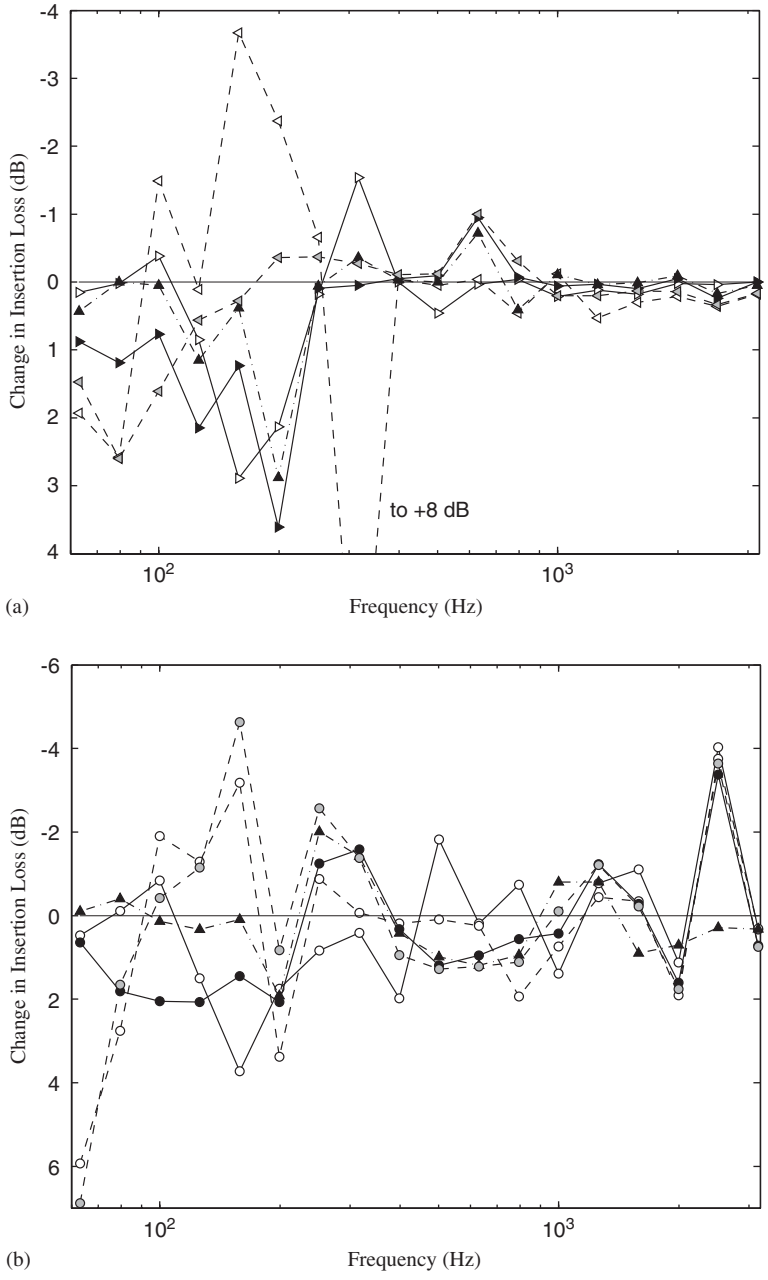

Fig. 14. Spectral comparison of different multiple-edge barrier designs over cutting of depth 0.4 m, see Fig. 2(a),(II);(b)(II). Key indicated in Fig. 12. Results are presented in terms of the change in insertion loss compared with a simple vertical, rigid barrier. Upper plot shows results for barrier (a)(II), solid line (–) with marker (▷) denotes results for (h) modification; dashed line (- -) with marker ◁ denote results for (j) modification; dash-dot line (-.) with marker (▲) denotes (ip) results; solid line (–) with marker (▶) denotes (hp) results; and dashed line (- -) with shaded triangle marker denotes (jp) modification results. Lower plot shows results for barrier (b)(II), lines denoted as above with circles replacing triangles save dash-dot line(-.) with (▲) denoting (ip) modification results.

varies its efficiency. Assuming that the panel in (j) is large enough to neglect energy diffracting around its lower edge, then the difference in performance of barrier (h) must be due to the introduction of the horizontal section. The central stanchion of the barrier and the horizontal section were then modelled with absorbing treatment as shown in design (hp). The absorbing coating corresponds to treatment α_2 as described in Fig. 3 and is intended to simulate a mineral wool panel. This resulted in an increase in insertion loss for barrier (hp); the design was of equal efficiency to (jp) barrier above 300 Hz. Note that the (h) design here does not work efficiently in the lower-frequency range. This is due to resonance in the open cavity, which after placing an absorptive panel in the cavity, (hp), is considerably damped.

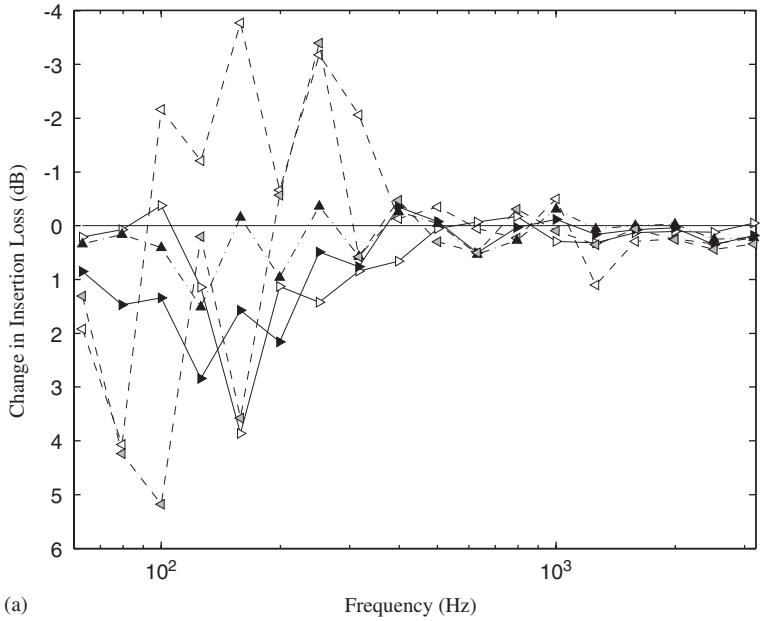

(a)

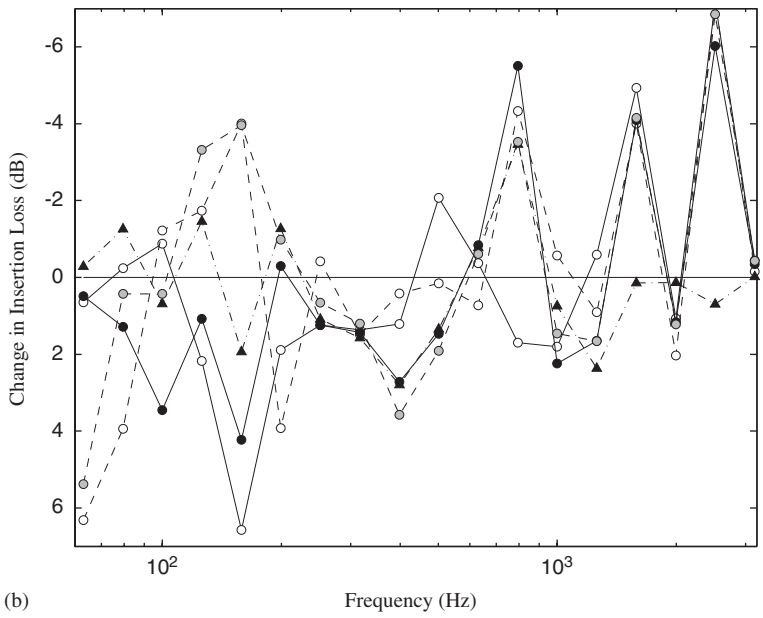

(b)

Fig. 15. Spectral comparison of different multiple-edge barrier designs over cutting of depth 1.0 m, see Fig. 2(a),(III);(b)(III). Key indicated in Fig. 12. Results are presented in terms of the change in insertion loss compared with a simple, vertical, rigid barrier. Line codes and markings are the same as Fig. 14.

Applying the same design to barriers with the source situated in a cutting is shown in Figs. 14 and 15 to be compared with insertion loss spectra in Fig. 7. Fig. 14 shows the spectral effects of adding a horizontal section joining the extra panel to the screen and of applying absorbing qualities to certain sections with source located over 0.4 m deep cutting. The receiver position is 40 m from the barrier and 1.5 m above the ground surface, and the results are presented in terms of the change in insertion loss compared with those for a rigid screen (i) (design (a)(II) in Fig. 2). For each modification of design (i) there is a marginal, but positive, difference in insertion loss at low frequencies ($\leqslant 200$ Hz) except the (j) design which shows some significant variability and is interpreted as resulting from interference effects since this is not observed in the spectrum for absorbent barrier (jp). Absorbing treatment was modelled primarily to reduce the effects of reflections between the vertical faces of the multiple-edged barriers. In fact, a comparison of the results for designs (hp) and (jp) suggests that the difference is small. However, when the screen is brought closer to the source, modifications of the screen design, Fig. 2(b)(II), the change in insertion loss compared with the rigid screen, design (i) is variable. It can be concluded that adding absorptive treatment in design (hp) changes the insertion loss significantly against its rigid counterpart (h) in certain frequency bands but the overall effect is negligible. Fig. 15 presents the changes in insertion loss, compared to simple design results Fig. 7. It must be emphasised here that a single barrier has a negative relative effect over sound attenuation compared to grassland above 300 Hz as shown in Fig. 7. Nevertheless, apart from design (j), all modification designs in this class are slightly more effective than an unmodified single rigid, vertical screen.

Finally, the case combining two single-barrier foundations which worked effectively for flat grassland case is illustrated in Fig. 16. It is difficult to make general conclusions from the spectral analysis but a notable observation is that positive changes in insertion loss occur, over single foundation design, for both cutting geometries if absorbent material is added to front panels of the screen design. A significant increase in effectiveness for the double barrier and 0.4 m deep cutting up to around 300 Hz. Meanwhile the effectiveness of the absorbent double-barrier configuration for 1.0 m cutting is consistently favourable up to 800 Hz. The rigid design also shows some promise except at a single frequency, 160 Hz.

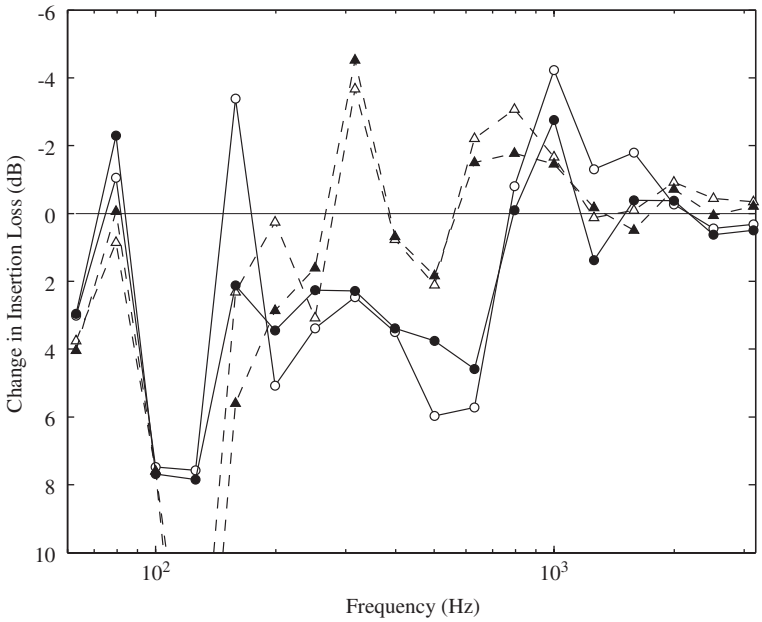

Fig. 16. Spectral comparison of double-barrier configuration over cuttings of depth 0.4 and 1.0 m, see Fig. 2(a) with (b),(II-III). Key indicated in Fig. 12(aa). Results are presented in terms of the change in insertion loss compared with simple vertical, rigid barriers, (a) with short screen (b). Dashed line (- -) with marker (△) denotes results for double rigid barrier adjacent to 0.4 m deep cutting; solid line (–) with marker (○) denotes results for double rigid barrier adjacent to 1.0 m cutting; solid markers denote respective results with source-facing absorbent material.

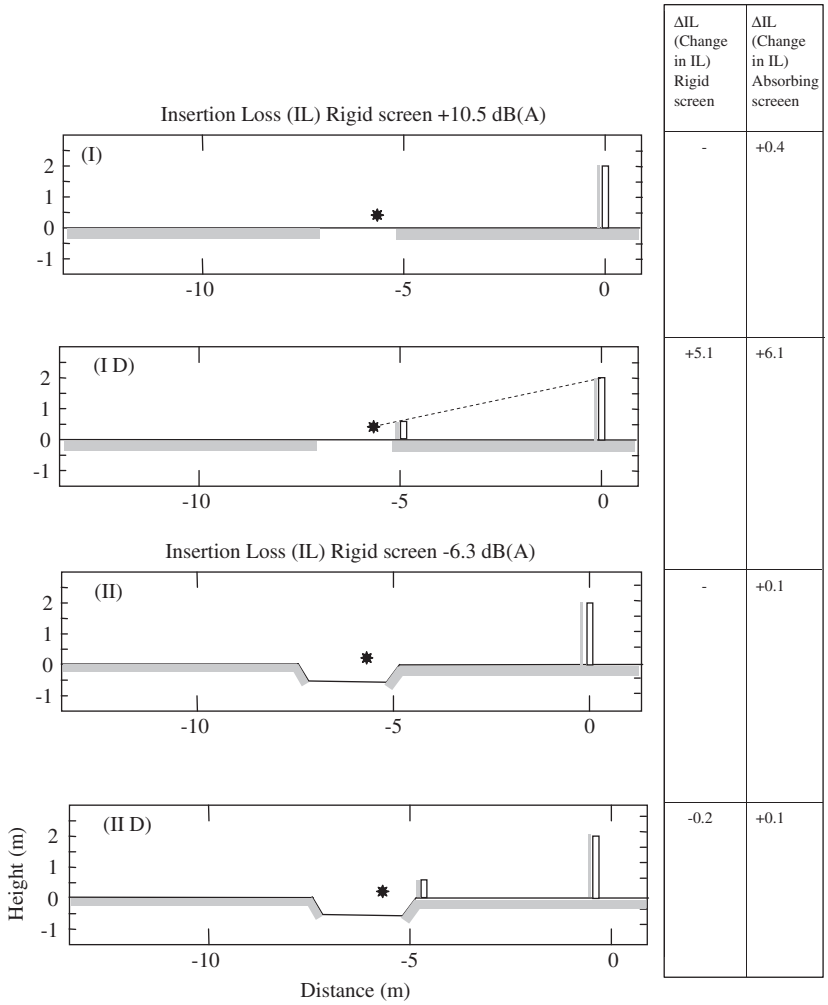

Fig. 17. Comparison of single and double rigid/absorbing barriers for flat ground and 0.4 m deep cutting. Results are in terms of average insertion loss over six given points. Plots show the location of absorbing material, on an otherwise rigid screen.

Results for double-barrier configuration are summarised as average insertion loss values over six receiver positions and a broadband traffic noise spectrum in Fig. 17. Averaging over the positions 20, 40, 80 m with heights 1.5 and 4.5 m it is clear from the figure that an additional small screen nearer the source has a benefit for traffic noise over flat grassland. However, an additional screen has little effect when the source is located in a highway cutting. In fact it may be worthwhile to use a single short barrier close to the cutting, see Fig. 7.

4. Conclusions

In this paper, the problem of acoustic propagation from a coherent line source within a cutting of arbitrary cross-section and surface impedance out over a noise barrier onto homogeneous absorbing ground has been studied using the boundary element method, Ref. [1].

The scope of the numerical scheme to provide predictions of practical interest has been demonstrated by computations for a broad-band traffic noise spectrum of propagation from a vehicle source located at 0.5 m above the rigid floor of the cutting out onto surrounding flat ground. The significant effects of varying cutting

depth and of varying the geometry of the barrier to suit the non-flat ground type have been described. The results of the boundary element calculations lead to the following conclusions:

1. The ground geometry in the immediate vicinity of a noise source, such as a vehicle sitting in a cutting, can significantly effect the sound attenuation beyond a traffic highway.
2. Obstruction of sound propagation, by screens for example, from sources in cuttings can have a negative effect on attenuation.
3. A short noise barrier located *near* to a cutting may be more efficient than a taller barrier located *further* from a highway cutting. However, modifications of noise barrier designs located *near* and *far* from the source in cuttings have little effect on sound attenuation beyond the barrier foundations.
4. Double-barrier configurations can be extremely efficient in attenuating road traffic noise for flat ground. However, for non-flat topography it is difficult to make such conclusions. Scale model and field measurements are necessary to make conclusions. Laboratory measurements at MWL, KTH, Stockholm to test the efficiency of multi-edged screens, with sources located in small cuttings, will soon take place and field measurements are planned. In the future stronger conclusions may be drawn for numerical predictions that have been validated against physical data.

Acknowledgements

The author acknowledges Prof. S.N. Chandler-Wilde, Department of Mathematics, University of Reading, UK in the development of the boundary element method and Prof. M Åbom, MWL, KTH, Stockholm for technical discussions.

References

[1] A.T. Peplow, Numerical predictions of sound propagation from a cutting over a surrounding flat ground, *Journal of Computational Acoustics* 13 (1) (2005) 145–162.
[2] D. Duhamel, Efficient calculation of the three-dimensional sound pressure field around a noise barrier, *Journal of Sound and Vibration* 197 (5) (1996) 547–571.
[3] S.N. Chandler-Wilde, Tyndall Medal Lecture: the boundary element method in outdoor noise propagation, in: *Proceedings of the Institute of Acoustics*, Vol. 19, 1997, pp. 27–50.
[4] D.C. Hothersall, S.N. Chandler-Wilde, N.M. Hajmirzae, Efficiency of single noise barriers, *Journal of Sound and Vibration* 146 (1991) 303–322.
[5] P.A. Morgan, Boundary Element Modelling and Full Scale Measurement of the Acoustic Performance of Outdoor Noise Barriers, PhD Thesis, Brunel University, 1999.
[6] D.H. Crombie, D.C. Hothersall, S.N. Chandler-Wilde, Multiple-edge noise barriers, *Applied Acoustics* 44 (1995) 353–367.
[7] G.R. Watts, Acoustic performance of multiple edge noise profile at motorway sites, *Applied Acoustics* 47 (1996) 47–66.
[8] G.R. Watts, P.A. Morgan, Acoustic performance of an interference-type noise-barrier profile, *Applied Acoustics* 49 (1996) 1–16.
[9] A.T. Peplow, S.N. Chandler-Wilde, Noise propagation from a cutting of arbitrary cross-section and impedance, *Journal of Sound and Vibration* 146 (1999) 303–322.
[10] G.R. Watts, Effectiveness of shallow cuttings in controlling road traffic noise, TRL Unpublished Report, PR/SE/213/96. Transport Research Laboratory, Crowthorne, UK, 1997.
[11] S.N. Chandler-Wilde, D.C. Hothersall, Efficient calculation of the Green-function for acoustic propagation over a homogeneous impedance plane, *Journal of Sound and Vibration* 180 (1995) 705–724.
[12] K.B. Rasmussen, The effect of terrain profile on sound propagation outdoors, Report Number 111, Danish Acoustical Institute, 1982.
[13] P.J.T. Filippi, Extended sources radiation and Laplace type integral representation: application to wave propagation above and within layered media, *Journal of Sound and Vibration* 91 (1983) 65–84.
[14] D. Habault, Sound propagation above an inhomogeneous plane: boundary integral equation methods, *Journal of Sound and Vibration* 100 (1985) 55–67.
[15] D.H. Crombie, D.C. Hothersall, The performance of multiple noise barriers, *Journal of Sound and Vibration* 176 (4) (1994) 459–473.
[16] L. Nordin, Studies of barriers and the influence of soft edge, shape and wind, TRITA–KTH 2000:35 IISN 1103-470X, 2000.
[17] M.E. Delany, E.N. Bazley, Acoustical properties of fibrous absorbent materials, *Applied Acoustics* 3 (1970) 105–116.